2014 American Control Conference (ACC)
June 4-6, 2014. Portland, Oregon, USA

Range Extension Control System for Electric Vehicles by LTI Modeling with Generalized Frequency Variable

Yafei Wang, Hiroshi Fujimoto, and Shinji Hara

Abstract— **Electric vehicles (EVs) have been identified as being alternatives to traditional engine vehicles due to their reduced impact on environments. However, as one of the inherent disadvantages, limited operating range prevents EVs from wide spreading. Although high efficiency motors and large-size batteries can be employed to increase mileage per charge, pure control approaches for cruising range extension are more interesting and promising. For EVs equipped with front and rear in-wheel-motors, the cruising range can be extended by optimal torque distribution among all the wheels. On the other hand, an increasing number of control functions are desired for EVs. For example, control systems for safety, comfort and economy have been developed and utilized in the recent decades. Nevertheless, too many control functions exert heavy processing burden on the onboard control unit. In this paper, by modeling an EV as a LTI system with generalized frequency variables, a new control concept is proposed to extend cruising range, in which the process task is distributed to subsystems and the burden of the central controller can be released. Moreover, the stability criteria are established for the controller design, and the proposed range extension control system is verified by simulation.**

I. Introduction

Electric vehicles (EVs), as green solutions for future transportation, are gaining an increasing concern from both industry and academic fields. However, limited cruising range per charge prevents EVs from public recognition in a certain extent. An intuitive solution for this issue is to increase the size of onboard battery, but additional space is required. Moreover, the cost and weight are increased, which render it unpractical in many cases. Some other methods focus on charging infrastructures, for example, optimal quick charge station arrangement and the concept of wireless charging while driving were proposed [1]-[2]. Along with the development of motors, the energy of EVs can be utilized more effectively and the cruising range is increased accordingly [3]. Nevertheless, the aforementioned approaches need additional hardware or facilities. Meanwhile, pure control algorithms to increase mileage per charge were studied in the past few years. In [4], torque distribution strategy is studied by Yuan *etc*. for a front-and-rear-wheel-driven EV, and NEDC driving cycle was employed to demonstrate the effectiveness of the proposed method on a test bench. A load transferring and slip ratio controller was studied for front-rear-independent-driven EVs during acceleration and braking [5]. The strategy optimizes distribution ratio of driving/braking torques on front and rear wheels, and the energy consumption was shown to be reduced by 30%. A latest research worked on torque management for EVs with in-wheel-motors (IWMs) [6], and the experiments demonstrated a 0.9 km increase per 1 kWh compared with the non-control case. The proposed controller is named as range extension control system (RECS). It should be noted that these algorithms are designed in a central control manner.

Meanwhile, an increasing number of control functions are desired for advanced performances of EVs related with safety, comfort and economy [7]. If all of these functions are implemented in a central processor, the complexity and processing load are increased considerably [8]. As an alternative, distributed control is an ideal solution to such problems. Proposed by Hara *etc*., a formation control methodology was investigated for multiple homogeneous dynamic agents which are locally stabilized by identical controllers [9]-[11]. One of the main contributions of this literature is the establishment of a stability criterion for a linear system with generalized frequency variables. They first introduced the notion: assume a large scale system is denoted by $L(s)$, and the transfer function's 's' variable is replaced with a rational function '$\phi(s)$', and $G(s)$ is defined as $L(\phi(s))$. Then, Lyapunov stability of multi-agent coordination is transformed to observing the relationship between the pole locations of $L(s)$ and the region of $\phi(s)$ in the complex plane. Based on this concept, four wheels of an EV can be treated as four agents, and each of them is controlled by an inverter, i.e., an in-wheel-motor together with an inverter form an agent. Moreover, the agents are commanded by a central controller to achieve the goal of range extension. However, even if the local system is stable, stability of the overall system cannot be guaranteed. In this paper, by modeling the EV and local agents as a LTI system and generalized frequency variables, respectively, system stability criteria are studied. The proposed RECS is verified by simulation.

II. System Description and Modeling

A. System Description

As aforementioned, an EV with four IWMs can be seen as a control system with four agents. The overall system is illustrated in Fig. 1, where green lines stand for information flow and brown lines represent energy flow. The central controller works as a coordinator and the four wheels are manipulated by the inverters. The global coordinator calculates required torques based on driver's command and other necessary information and then sends torque commands

Y. Wang is with the Department of Advanced Energy, Graduate School of Frontier Sciences, The University of Tokyo, Chiba, Japan (phone: 04-7136-3873; fax: 04-7136-3847; e-mail: wang@hori.k.u-tokyo.ac.jp).

H. Fujimoto is with the Department of Advanced Energy, Graduate School of Frontier Sciences, The University of Tokyo, Chiba, Japan (e-mail: fujimoto@ k.u-tokyo.ac.jp).

S. Hara is with the Department of Information Physics and Computing, The University of Tokyo, 7-3-1 Hongo, Bunkyo-ku, Tokyo, Japan. (e-mail: shinji_hara@ipc.i.u-tokyo.ac.jp).

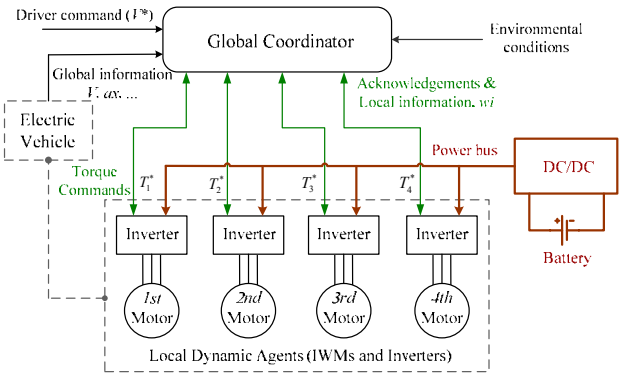

Fig. 1. Diagram of the overall system.

to the inverters to control IWMs. It should be mentioned that, because of such structure (both global and local controllers exist), it is possible to implement RECS using the proposed approach discussed in the following sections.

B. Vehicle Dynamics

Vehicle model is explained in this subsection, and it is illustrated in Fig. 2 together with a single wheel model. The system can be described as

$$J_i \cdot \dot{\omega}_i = T_i - F_i \cdot r \tag{1}$$

$$\left(M + \sum_{i=1}^{4} \frac{J_i}{r^2} \right) \cdot \dot{V} = \sum_{i=1}^{4} F_i - F_{dr} \tag{2}$$

$$F_{dr} = \mu \cdot M \cdot g + \frac{1}{2} \cdot k_{ad} \cdot V^2 \tag{3}$$

$$V_{\omega_i} = \omega_i \cdot r \tag{4}$$

where i reprents the ith wheel, and it is a number from 1 to 4, J_i, $V_{\omega i}$ and ω_i are the wheel's inertial, velocity and angular velocity, respectively, V is vehicle's velocity, T_i is the torque applied to the wheel, F_i is the driving force, F_{dr} is resistance force which includes rolling resistance and air resistance, μ and k_{ad} are the coefficient for rolling and air drag resistances, respectively, M is vehicle mass, r is the radius of the wheels.

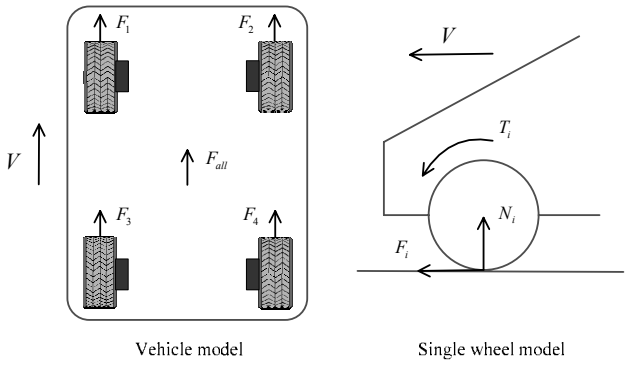

Fig. 2. Vehicle model and single wheel model.

For the single wheel model, an importance concept is slip ratio, and it is defined as Eq. (5) by considering both acceleration and deceleration cases.

$$\lambda_i = \frac{V_{\omega_i} - V}{\max(V_{\omega_i}, V)} \tag{5}$$

Moreover, friction coefficient between tire and road is a function of λ_i, and the driving force can be represented as

$$F_i = \mu_i(\lambda_i) \cdot N_i \tag{6}$$

Furthermore, to facilitate the following discussion, driving stiffness D_s is introduced into Eq. (6) by assuming a linear relationship between λ_i and μ_i, as

$$F_i = D_s \cdot N_i \cdot \lambda_i \tag{7}$$

$$D_s := \frac{\partial \mu_i}{\partial \lambda_i}\Big|_{\lambda_i = 0} \tag{8}$$

One of the most important factors that can be utilized for torque distribution is load transfer caused by acceleration and deceleration, and the normal forces are expressed as

$$N_{1,2}(a_x) = \frac{M}{2 \cdot l}\left(l_r \cdot g - h_g \cdot a_x \right) \tag{9}$$

$$N_{3,4}(a_x) = \frac{M}{2 \cdot l}\left(l_f \cdot g + h_g \cdot a_x \right) \tag{10}$$

where l_f and l_r are the distance from center of gravity (CoG) to front and rear wheels, respectively, l is the sum of l_f and l_r, g is gravitational acceleration, a_x is vehicle's longitudinal acceleration/deceleration rate, and h_g is the height of CoG.

C. Torque Distribution Model

As aforementioned, the commanded torque of the driver can be distributed to four wheels to save energy, and a simple model is explained here. The total driving force of a vehicle is the sum of the driving forces of all the wheels. Therefore, the driving force at each wheel can be set differently to achieve a desired operation point in real time, as long as the total driving force matches the driver's force requirement. The driving force at each wheel is defined as

$$F_1 = F_2 = \frac{1}{2} \cdot (1 - k) \cdot F_{all} \tag{11}$$

$$F_3 = F_4 = \frac{1}{2} \cdot k \cdot F_{all} \tag{12}$$

where k represents distribution ratio between front two and rear two wheels, and it will be designed based on weight transfer during acceleration and deceleration. From Eqs. (11) and (12), the forces of the front two wheels are evenly distributed, and so are the rear two wheels. Moreover, k =0 means front drive only, and k =1 means rear drive only. In the next section, it will be shown that a proper k can minimize the total output torque while maintaining desired velocity.

III. Torque Distribution Law

In this section, given the pattern of vehicle velocity, an optimal distribution ratio k_{opt} is designed to minimize the total output of motors, i.e., the efficiency between the total motor output and total driving force is optimized. First, the wheel torques can be given as Eqs. (13) and (14) by ignoring inertial torques. As wheel torque is dominated by the torque of driving force (in the case of wheel adhesion), this assumption is reasonable.

$$T_{1,2} = F_{1,2} \cdot r = \frac{r}{2} \cdot (1-k) \cdot F_{all} \tag{13}$$

$$T_{3,4} = F_{3,4} \cdot r = \frac{r}{2} \cdot k \cdot F_{all} \tag{14}$$

$$T_{all} = T_1 + T_2 + T_3 + T_4 \tag{15}$$

The total motor output is obtained by the summation of motor output at each wheel.

$$P_{out} = \sum_{i=1}^{4} P_{out,i} = \sum_{i=1}^{4} T_i \cdot \omega_i \tag{16}$$

Then, considering wheel angular velocity has two expressions in terms of acceleration and deceleration, the optimal distribution ratio is explained separately as discussed below.

A. Acceleration

In case of acceleration, wheel angular velocity is given as below based on Eq. (5).

$$\omega_i = \frac{V}{r} \cdot \frac{1}{1-\lambda_i} \tag{17}$$

Moreover, from Eqs. (7), (11) and (12), slip ratios can be expressed as

$$\begin{aligned} \lambda_1 = \lambda_2 &= \frac{(1-k) \cdot F_{all}}{2 \cdot D_s \cdot N_f} \\ \lambda_3 = \lambda_4 &= \frac{k \cdot F_{all}}{2 \cdot D_s \cdot N_r} \end{aligned} \tag{18}$$

By inserting Eqs. (17) and (18) into Eq. (16), P_{out} is transformed to

$$P_{out} = F_{all} \cdot V \cdot \left(\sum_{i=1}^{2} \frac{1-k}{2 \cdot (1-\lambda_i)} + \sum_{i=3}^{4} \frac{k}{2 \cdot (1-\lambda_i)} \right) \tag{19}$$

and the optimal ratio k_{opt} is finally obtained as Eq. (20) by solving the partial differential equation $\partial P_{out} / \partial k_{opt} = 0$.

$$k_{opt}(a_x) = \frac{\sum_{i=3}^{4} N_i(a_x)}{\sum_{i=1}^{2} N_i(a_x) + \sum_{i=3}^{4} N_i(a_x)} \tag{20}$$

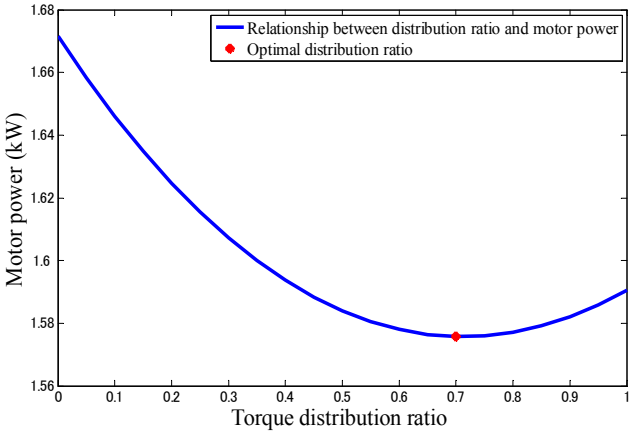

Fig. 3. Total motor output vs. torque distribution ratio.

B. Deceleration

Wheel angular velocity is given as Eq. (21) based on Eq. (5) in case of deceleration.

$$\omega_i = \frac{V}{r_i} \cdot (1+\lambda_i) \tag{21}$$

and the slip ratios are also given in Eq. (18). Then, P_{out} is transformed as

$$P_{out} = F_{all} \cdot V \cdot \left(1 + \sum_{i=1}^{2} \frac{\lambda_i}{2} + k_{opt} \cdot \left(\sum_{i=3}^{4} \frac{\lambda_i}{2} - \sum_{i=1}^{2} \frac{\lambda_i}{2} \right) \right) \tag{22}$$

Similar to the acceleration case, the optimal ratio k_{opt} can be calculated by solving the partial differential equation $\partial P_{out} / \partial k_{opt} = 0$. Interestingly, the optimal distribution ratio of deceleration has the same form as the acceleration case, which facilitates the overall system design.

To demonstrate this concept, based on the parameters given in [12], assume that the EV accelerates at 0.2 g and reaches 30 km/h, the required power can be represented as a function of distribution ratio based on Eq. (19), which is shown as Fig. 3. The red dot in Fig. 3 is the optimal ratio that minimizes motor power.

IV. Controller Design and Stability Analysis

After the torque distribution law is established, realization of torque control at each wheel should be considered, and the stability analysis is also necessary.

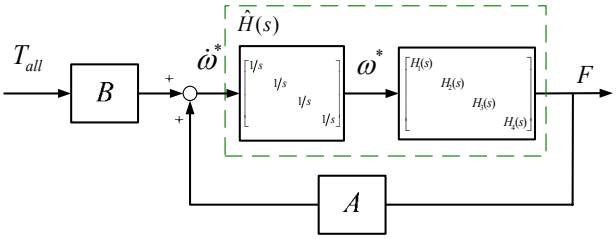

Fig. 4. Block diagram of the overall system.

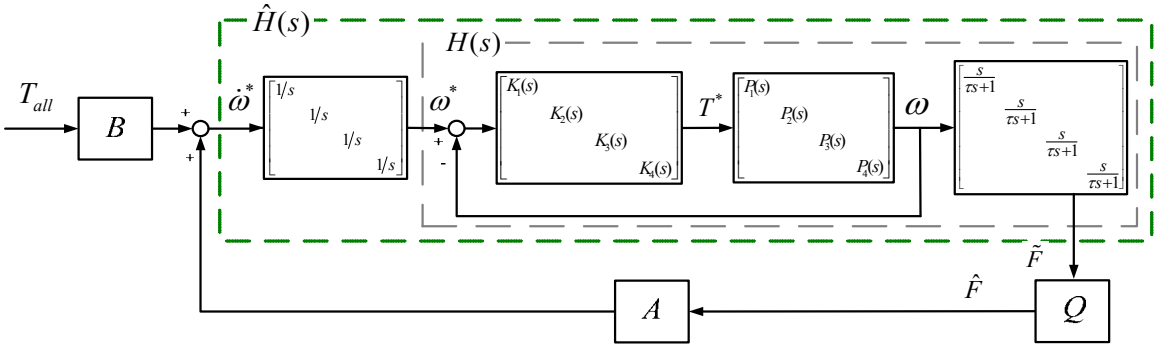

Fig. 5. Detailed representation of the overall control system.

A. Controller Design for RECS

From Eq. (1), derivative of wheel angular velocity is obtained as Eq. (23).

$$\dot{\omega}_i = \frac{1}{J_i}(T_i - F_i \cdot r) \tag{23}$$

For four wheels, a state space equation can then be constructed as Eq. (24) based on Eqs. (13), (15) and (23).

$$\dot{\omega} = A \cdot F + B \cdot T_{all} \tag{24}$$

where

$$\omega = \left[\omega_1,\ \omega_2,\ \omega_3,\ \omega_4\right]^T, F = \left[F_1,\ F_2,\ F_3,\ F_4\right]^T,$$
$$A = \mathrm{diag}\left(\frac{-r}{J_1},\ \frac{-r}{J_2},\ \frac{-r}{J_3},\ \frac{-r}{J_4}\right),$$
$$B = \left[\frac{1-k}{2\cdot J_1},\ \frac{1-k}{2\cdot J_2},\ \frac{k}{2\cdot J_3},\ \frac{k}{2\cdot J_4}\right]^T.$$

That is, the overall system has a structure as Fig. 4, where $H_i(s)$ represents the local dynamic agent which includes a wheel and its controller. From Fig. 4, it can be observed that the input to $H_i(s)$ is the reference of wheel angular velocity and the output is the driving force at the ith wheel. Detailed description of the system is illustrated in Fig. 5.

As can be seen in Fig. 4, driving forces are required to construct the feedback loops. However, they are difficult to be measured directly. In this research, Driving Force Observer (DFO) is employed to estimate the forces [12]. The force estimation without filtering is represented as

$$\hat{F}_{d,i} = \Delta_{Q,i} \cdot \omega_i \cdot s \tag{25}$$

$$\text{where}\quad \Delta_{Q,i} = \begin{cases} \dfrac{r\cdot M\cdot(1-k)}{2}, & i = 1,2 \\ \dfrac{r\cdot M\cdot k}{2}, & i = 3,4 \end{cases}$$

For four wheels, DFOs can be rearranged as Eq. (26) by taking the LPFs into account, where Q is defined as a diagonal matrix diag($\Delta_{Q,1}$, $\Delta_{Q,2}$, $\Delta_{Q,3}$, $\Delta_{Q,4}$). It can be observed that DFO can be divided into dynamic part and parameter part.

$$\hat{F} = \left[\hat{F}_1,\ \hat{F}_2,\ \hat{F}_3,\ \hat{F}_4\right]^T = \left[\hat{F}_{d,1},\ \hat{F}_{d,2},\ \hat{F}_{d,3},\ \hat{F}_{d,4}\right]^T \cdot \frac{1}{\tau\cdot s+1}$$
$$= Q\cdot\left[\omega_1,\ \omega_2,\ \omega_3,\ \omega_4\right]^T \cdot \frac{s}{\tau\cdot s+1} \tag{26}$$

Then, Eq. (27) can be obtained from Eqs. (1) and (2).

$$\sum_{i=1}^{4} T_i = \sum_{i=1}^{4}\left(J_i\cdot\dot{\omega}_i\right) + \left(M\cdot r^2 + \sum_{i=1}^{4} J_i\right)\cdot\dot{\omega}_i \tag{27}$$

For the ith wheel, the plant can then be nominalized as

$$P_i(s) = \frac{\omega_i}{T_i} = \frac{1}{\left(\dfrac{M\cdot r^2}{4} + 2\cdot J_i\right)\cdot s} := \frac{1}{\Delta_{G,i}\cdot s} \tag{28}$$

Assume wheel velocity is controlled by a *PI*-controller, inner-loop transfer function $H_i(s)$ in Fig. 5 is then derived as

$$H_i(s) = \frac{\left(K_P\cdot s + K_I\right)\cdot s}{\left(\Delta_{G,i}\cdot s^2 + K_P\cdot s + K_I\right)\cdot\left(\tau\cdot s+1\right)} \tag{29}$$

where K_P and K_I are the proportional and integral gains. Moreover, $\hat{H}_i(s)$ is defined as $H_i(s)/s$.

B. Stability Analysis

From Fig. 5, $G(s)$ from T_{all} to $\tilde{F}$ is obtained as

$$G(s) = \left(\frac{1}{\hat{H}(s)}\cdot I_n - A\cdot Q\right)^{-1}\cdot B = \mathcal{F}_u\left(\begin{bmatrix} A\cdot Q & B \\ I_n & 0 \end{bmatrix},\ \hat{H}(s)\cdot I_n\right) \tag{30}$$

where $\mathcal{F}_u$ denotes the upper linear fractional transformation, and $\hat{H}(s)$ is used to represent $\hat{H}_i(s)$ as the four wheels have the same dynamics. Consider a transfer function in the form of $L(s) = \left(s\cdot I_n - A\cdot Q\right)^{-1}\cdot B$, the following equations exist

$$G(s) = L\left(\phi(s)\right),\quad \phi(s) := 1/\hat{H}(s) \tag{31}$$

As can be observed, the transformed transfer function $G(s)$ can be seen to have a generalized frequency variable $\phi(s)$.

Moreover, define the domains Ω_+ and Ω_+^c in the complex plane as

$$\Omega_+ := \phi(C_+), \quad \Omega_+^c := C \setminus \Omega_+ \tag{32}$$

and then, the proposition made in [11] can be applied to the system as: $G(s) = L(\phi(s))$ is stable if and only if all the eigenvalues of $A \cdot Q$ are located in Ω_+^c. Detailed derivations can be found in [9]-[11]. In this application, $\phi(s)$ can be obtained as

$$\phi(s) = 1/\hat{H}(s) = \frac{(\tau \cdot s + 1) \cdot (\Delta_G \cdot s^2 + K_P \cdot s + K_I)}{K_P \cdot s + K_I}$$

$$:= \frac{c \cdot s^3 + d \cdot s^2 + e \cdot s + b}{a \cdot s + b} \tag{33}$$

Then, the domains Ω_+ and Ω_+^c can be characterized in the complex plane: consider that these regions are partitioned by the image of $\phi(j\omega)$ where $\omega \in R$, the real and imaginary parts of $\phi(j\omega)$ can be defined as follows ($f(\omega) := Re[\phi(j\omega)]$ and $g(\omega) := Im[\phi(j\omega)]$):

$$f(\omega) = \frac{-a \cdot c \cdot \omega^4 + (a \cdot e - b \cdot d) \cdot \omega^2 + b^2}{a^2 \cdot \omega^2 + b^2} \tag{34}$$

$$g(\omega) = \frac{(a \cdot d - b \cdot c) \cdot \omega^3 - b \cdot (a - e) \cdot \omega}{a^2 \cdot \omega^2 + b^2} \tag{35}$$

The intersecting points of $\phi(j\omega)$ and the imaginary axis can be calculated by finding ω_I which satisfies $f(\omega_I) = 0$ and then calculating $g(\omega_I)$. Similarly, the intersecting points of $\phi(j\omega)$ and the real axis can be determined from $f(\omega_R)$ where ω_R satisfies $g(\omega_R) = 0$. Here, ω_R and ω_I are given as Eqs. (36) and (37), where ω_I have two roots and ω_R have one or three roots depending on the existence of $\omega_R^{2,3}$.

$$\omega_R^1 = 0, \quad (\omega_R^{2,3})^2 = \frac{b \cdot (a - e)}{a \cdot d - b \cdot c} \tag{36}$$

$$(\omega_I^{1,2})^2 = \frac{(a \cdot e - b \cdot d) + \sqrt{(a \cdot e - b \cdot d)^2 + 4 \cdot a \cdot b^2 \cdot c}}{2 \cdot a \cdot c} \tag{37}$$

Inserting Eqs. (36) and (37) into Eqs. (34) and (35), respectively, it is known that $\phi(j\omega)$ has two intersecting points with imaginary axis. For real axis, the number of intersecting points is 3 if $\omega_R^{2,3}$ exist, otherwise the number is 1.

Two illustrative examples are provided here. The eigenvalues of $A \cdot Q$ are $-M \cdot r \cdot (1-k)/2$ and $-M \cdot r \cdot k/2$, where $k \in [0,1]$, and they range from -128.95 to 0 based on the parameters given in the Appendix. If the poles of local system are placed at -2.15±10.5i, as can be seen from Fig. 6 (a), the eigenvalues of $A \cdot Q$ are not in the scope of Ω_+^c. That is, the overall system is unstable even if local systems are stable. If the poles of the local system are placed at ±10, the eigenvalues of $A \cdot Q$ are in the domain of Ω_+^c as can be observed in Fig. 6 (b), which means the global system is stable.

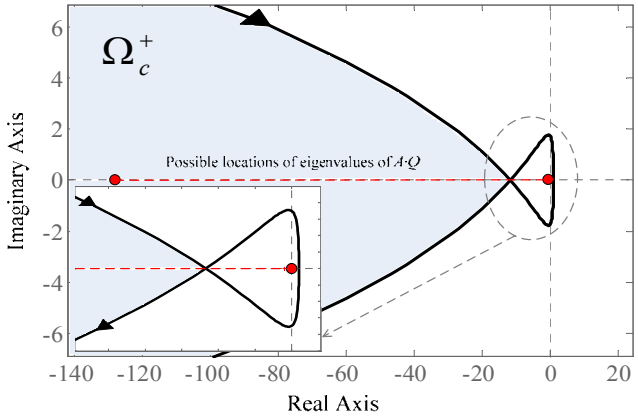

(a) Unstable example.

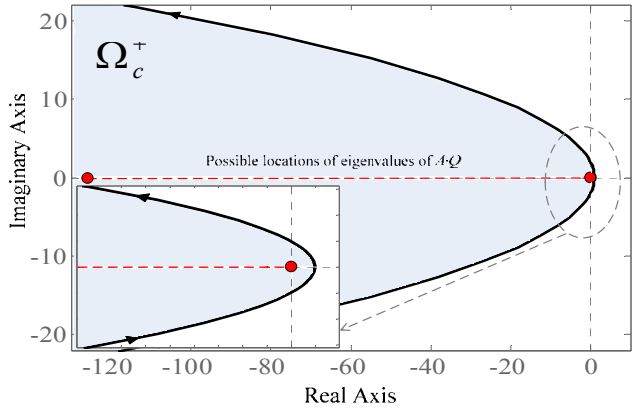

(b) Stable example.

Fig. 6. The eigenvalues of $A \cdot Q$ and the Ω_+^c domain.

V. Simulation

To evaluate the proposed range extension control system, based on the vehicle parameters provided in [12], simulations were conducted. Normally, vehicles are front-wheel-driven, rear-wheel-driven or even torque distribution between front and rear axles. Therefore, k was selected to be 0, 0.5 and 1 for comparison with the proposed optimal distribution ratio. The vehicle is assumed to run on a high friction road, and the driving stiffness D_s and resistance coefficient μ are set to 10 and 0.7, respectively. Considering that normal driving cycles are groups of several acceleration, constant-speed and deceleration patterns, a speed pattern is designed as: first accelerate at 0.25 g for 3.33 seconds, and then cruise for 3 seconds at a constant speed of 8.3 m/s, and finally decelerate at -0.25 g for 3.33 seconds, to evaluate energy saving performances. In addition, as the input to the proposed controller is the torque reference, a controller is designed to transform reference speed to reference torque. The figures of Fig. 7 illustrate simulation results. Fig. 7 (a) shows that all of the distribution ratios can guarantee velocity tracking performance. That is, the comparison is fair as all the speed patterns are the same. Fig. 7 (b) shows all the distribution ratios, in which the optimal k changes with time. Fig. 7 (c) gives the comparison of required input energy. As can be seen, the proposed method has the least energy consumption compared with the front-drive, rear-drive and 50:50 distribut-

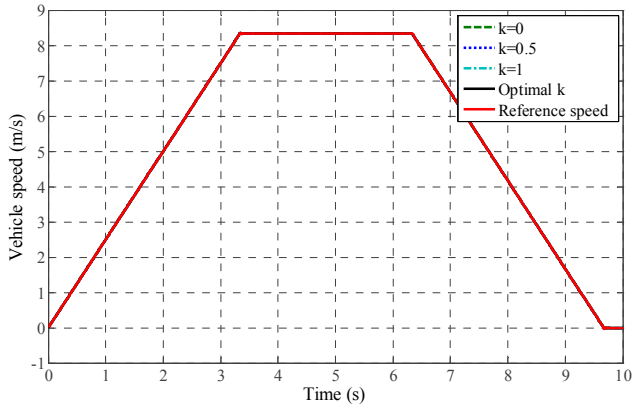

(a) Vehicle speed comparison.

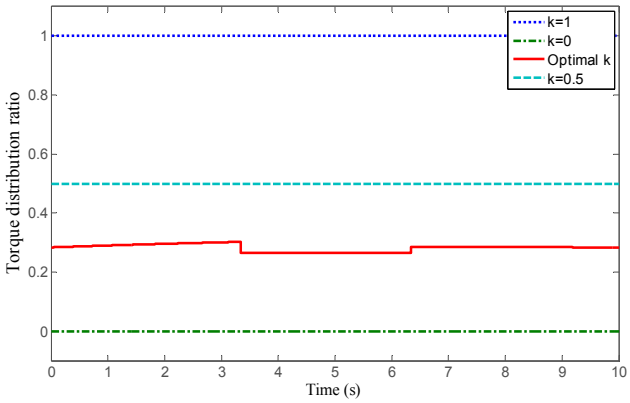

(b) Torque distribution ratio comparison.

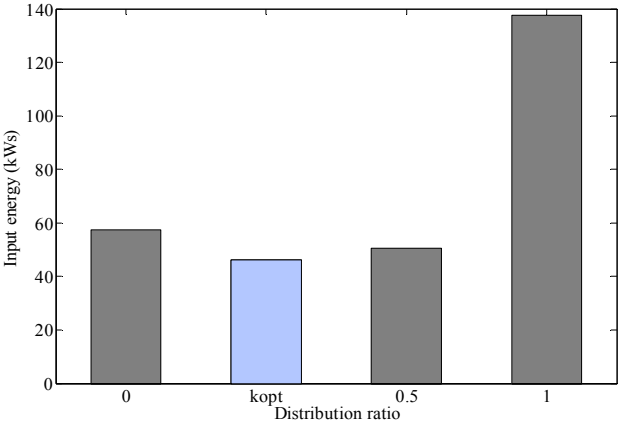

(c) Input energy comparison.

Fig. 7. Simulation results of different torque distribution ratios.

ion cases. Furthermore, the energy consumption of different cases are represented in terms of cruising range per kWh as given in Table I. Obviously, the proposed torque management method can drive the EV longer than other distribution ratios.

TABLE I
CRUISING RANGE COMPARISON

Distribution Ratio	0	0.5	1	k_{opt}
Cruising Range per kWh (km)	3.1	3.8	1.4	4.4

VI. CONCLUSIONS AND FUTURE WORKS

In this paper, a pure control methodology that distributes driving torque between front and rear axles is proposed to increase mileage per charge of EVs, and the proposed range extension control system is designed based on LTI modeling with generalized frequency variables. The benefits of such system are: 1) the process task is distributed to subsystems which release the burden of the central controller; 2) no additional hardware modification is required. Considering that two loops exit in such kind of control system, the stability criteria are established for the controller design. Currently, the torque distribution is designed based on weight transfer during acceleration/deceleration, and future works will take iron and copper losses into account for the derivation of distribution ratio and experiments will be conducted to verify the range extension performance.

REFERENCES

[1] Y. Hori, "application of electric motor, supercapacitor, and wireless power transfer to enhance operation of future vehicles," *in Proc. of IEEE Int. Symp. on Ind. Electron.*, Jul. 2010, pp.3633-3635.

[2] Z. Liu, F. Wen and G. Ledwich, "Optimal Planning of Electric-Vehicle Charging Stations in Distribution Systems," *IEEE Trans. Power Del.*, vol.28, no.1, pp.102-110, Jan. 2013.

[3] Y. G. Kim, C. B. Bae, J. M. Kim, and H. C. Kim, "Efficiency improvement by changeover of phase windings of multiphase permanent magnet synchronous motor with outer-rotor type," *in Proc of Twenty-Fifth Applied Power Electronics Conference and Exposition*, Feb. 2010, pp.112-119.

[4] X. Yuan, J. Wang, "Torque Distribution Strategy for a Front– and Rear–Wheel–Driven Electric Vehicle", *IEEE Trans. Veh. Technol.*, Vol. 61, No. 8, pp. 3365–3374, 2012.

[5] N. Mutoh, T. Kato, and K. Murakami, "Front-and-rear-wheel-independent-drive-type electric vehicle (FRID EV) taking the lead for next generation Eco-vehicles," *SAE Paper*, 2011-39-7206.

[6] S. Harada, and H. Fujimoto, "Range Extension Control System for Electric Vehicle on Acceleration and Deceleration Based on Front and Rear Driving/Braking Force Distribution Considering Slip Ratio and Motor Loss," *in Proc. of IEE of Japan Technical Meeting Record, IIC–10–019*, pp. 23–28, 2010. (in Japanese).

[7] Y. Hori, "Future vehicle driven by electricity and control-research on four wheel motored UOT electric March II," *IEEE Trans. Ind. Electron.*, vol. 51, no. 5, pp.954–962, Oct. 2004.

[8] D. Li, X. Shen and F. Yu, "Integrated vehicle chassis control with main/servo-loop structure," *Int. J. of Automotive Technology*, no.7, pp.803-812, 2006.

[9] S. Hara, H. Tanaka and T. Iwasaki, "Stability analysis of systems with generalized frequency variables," *IEEE Trans. on Autom. Control*, vol. 59, no. 2, Feb. 2014.

[10] H. Tanaka, S. Hara, and T. Iwasaki, "LMI stability condition for linear systems with generalized frequency variables," *in Proc. of the 7th Asian Control Conference*, 2009, pp. 136-141.

[11] S. Hara, T. Hayakawa, and H. Sugata, "LTI Systems with Generalized Frequency Variables: A Unified Framework for Homogeneous Multi-agent Dynamical Systems," *SICE J. of Control, Measurement, and System Integration*, vol. 2, no. 5, 2009.

[12] J. Amada and H. Fujimoto, "Torque based direct driving force control method with driving stiffness estimation for electric vehicle with in-wheel motor," *in Proc. of 38th IEEE-IECON*, 2012, pp.4904-4909.